Research Article | Vol. 7, No. 2 | 1 Feb 2017 | OPTICAL MATERIALS EXPRESS 555

Optical Materials EXPRESS

Thermal effects in systems of colloidal plasmonic nanoparticles in high-intensity pulsed laser fields [Invited]

V. S. GERASIMOV,[1] A. E. ERSHOV,[1,2,3] S. V. KARPOV,[1,3,4,*] A. P. GAVRILYUK,[1,2] V. I. ZAKOMIRNYI,[1,5] I. L. RASSKAZOV,[1,6] H. ÅGREN,[5] AND S. P. POLYUTOV[1]

[1]*Siberian Federal University, Krasnoyarsk 660041, Russia*
[2]*Institute of Computational Modeling, Federal Research Center KSC SB RAS, Krasnoyarsk 660036, Russia*
[3]*Siberian State Aerospace University, Krasnoyarsk 660014, Russia*
[4]*Kirensky Institute of Physics, Federal Research Center KSC SB RAS, Krasnoyarsk 660036, Russia*
[5]*Royal Institute of Technology, Stockholm SE-100 44, Sweden*
[6]*The Beckman Institute for Advanced Science and Technology, University of Illinois at Urbana-Champaign, Urbana, IL 61801, USA*
[*]*karpov@iph.krasn.ru*

Abstract: We have studied light induced processes in nanocolloids and composite materials containing ordered and disordered aggregates of plasmonic nanoparticles accompanied by their strong heating. A universal comprehensive physical model that combines mechanical, electrodynamical, and thermal interactions at nanoscale has been developed as a tool for investigations. This model was used to gain deep insight on phenomena that take place in nanoparticle aggregates under high-intensity pulsed laser radiation resulting in the suppression of nanoparticle resonant properties. Verification of the model was carried out with single colloidal Au and Ag nanoparticles and their aggregates.

OCIS codes: (160.4236) Nanomaterials; (250.5403) Plasmonics; (240.6680) Surface plasmons.

References and links

1. S. A. Maier, *Plasmonics: Fundamentals and Applications* (Springer Science & Business Media, 2007).
2. S. A. Maier, P. G. Kik, H. A. Atwater, S. Meltzer, E. Harel, B. E. Koel, and A. G. Requicha, "Local detection of electromagnetic energy transport below the diffraction limit in metal nanoparticle plasmon waveguide," Nature Materials **2**, 229–232 (2003).
3. R. Quidant, C. Girard, J.-C. Weeber, and A. Dereux, "Tailoring the transmittance of integrated optical waveguides with short metallic nanoparticle chains," Phys. Rev. B **69**, 085407 (2004).
4. A. Alu and N. Engheta, "Theory of linear chains of metamaterial/plasmonic particles as subdiffraction optical nanotrasmission lines," Phys. Rev. B **74**, 205436 (2006).
5. M. Février, P. Gogol, A. Aassime, R. Mégy, C. Delacour, A. Chelnokov, A. Apuzzo, S. Blaize, J.-M. Lourtioz, and B. Dagens, "Giant coupling effect between metal nanoparticle chain and optical waveguide," Nano Letters **12**, 1032–1037 (2012).
6. M. Stewart, C. Anderton, L. Thompson, I. Maria, S. Gray, J. Rogers, and R. Nuzzo, "Nanostructured plasmonic sensors," Chem. Rev. **108**, 494–521 (2008).
7. A. B. Evlyukhin, S. I. Bozhevolnyi, A. Pors, M. G. Nielsen, I. P. Radko, M. Willaten, and O. Alberktsen, "Detuned electrical dipoles for plasmonic sensing," Nano Letters **10**, 4571–4577 (2010).
8. G. Li, X. Li, M. Yang, M.-M. Chen, L.-C. Chen, and X.-L. Xiong, "A gold nanoparticles enhanced surface plasmon resonance immunosensor for highly sensitive detection of ischemia-modified albumin," Sensors **13**, 12794 (2013).
9. V. G. Kravets, F. Schedin, R. Jalil, L. Britnell, R. V. Gorbachev, D. Ansell, B. Thackray, K. S. Novoselov, A. K. Geim, A. V. Kabashin, and A. N. Grigorenko, "Singular phase nano-optics in plasmonic metamaterials for label-free single-molecule detection," Nature Materials **12**, 304–309 (2013).
10. N. S. Abadeer and C. J. Murphy, "Recent Progress in Cancer Thermal Therapy Using Gold Nanoparticles," The Journal of Physical Chemistry C **120**, 4691–4716 (2016).
11. J. C. Ndukaife, V. M. Shalaev, and A. Boltasseva, "Plasmonics - turning loss into gain," Science **351**, 334–335 (2016).

#279883 http://dx.doi.org/10.1364/OME.7.000555
Journal © 2017 Received 1 Nov 2016; revised 12 Dec 2016; accepted 15 Dec 2016; published 25 Jan 2017

Optical Materials EXPRESS

12. L. Hirsch, R. Stafford, J. Bankson, S. Sershen, B. Rivera, R. Price, J. Hazle, N. J. Halas, and J. West, "Nanoshell-mediated near-infrared thermal therapy of tumors under magnetic resonance guidance," Proceedings of the National Academy of Sciences **100**, 13549–13554 (2003).
13. S. Hashimoto, D. Werner, and T. Uwada, "Studies on the interaction of pulsed lasers with plasmonic gold nanoparticles toward light manipulation, heat management, and nanofabrication," Journal of Photochemistry and Photobiology C: Photochemistry Reviews **13**, 28 – 54 (2012).
14. E. Y. Lukianova-Hleb, X. Ren, R. R. Sawant, X. Wu, V. P. Torchilin, and D. O. Lapotko, "On-demand intracellular amplification of chemoradiation with cancer-specific plasmonic nanobubbles," Nature medicine **20**, 778–784 (2014).
15. A. Lenert, D. M. Bierman, Y. Nam, W. R. Chan, I. Celanović, M. Soljačić, and E. N. Wang, "A nanophotonic solar thermophotovoltaic device," Nature nanotechnology **9**, 126–130 (2014).
16. U. Guler, V. M. Shalaev, and A. Boltasseva, "Nanoparticle plasmonics: going practical with transition metal nitrides," Materials Today **18**, 227 – 237 (2015).
17. M. L. Brongersma, N. J. Halas, and P. Nordlander, "Plasmon-induced hot carrier science and technology," Nature nanotechnology **10**, 25–34 (2015).
18. G. Baffou, P. Berto, E. B. Ureña, R. Quidant, S. Monneret, J. Polleux, and H. Rigneault, "Photoinduced heating of nanoparticle arrays," ACS Nano **7**, 6478–6488 (2013).
19. A. D. Phan, T.-L. Phan, and L. M. Woods, "Near-field heat transfer between gold nanoparticle arrays," Journal of Applied Physics **114**, 214306 (2013).
20. P. Berto, M. S. A. Mohamed, H. Rigneault, and G. Baffou, "Time-harmonic optical heating of plasmonic nanoparticles," Phys. Rev. B **90** (2014).
21. A. O. Govorov and H. H. Richardson, "Generating heat with metal nanoparticles," Nano Today **2**, 30–38 (2007).
22. A. P. Gavrilyuk and S. V. Karpov, "Processes in resonant domains of metal nanoparticle aggregates and optical nonlinearity of aggregates in pulsed laser fields," Appl. Phys. B **97**, 163–173 (2009).
23. B. S. Luk'yanchuk, A. E. Miroshnichenko, M. I. Tribelsky, Y. S. Kivshar, and A. R. Khokhlov, "Paradoxes in laser heating of plasmonic nanoparticles," New Journal of Physics **14**, 093022 (2012).
24. A. E. Ershov, A. P. Gavrilyuk, S. V. Karpov, and P. N. Semina, "Optodynamic phenomena in aggregates of polydisperse plasmonic nanoparticles," Appl. Phys. B **115**, 547–560 (2014).
25. V. S. Gerasimov, A. E. Ershov, A. P. Gavrilyuk, S. V. Karpov, H. Ågren, and S. P. Polyutov, "Suppression of surface plasmon resonance in au nanoparticles upon transition to the liquid state," Opt. Express **24**, 26851–26856 (2016).
26. A. Alabastri, S. Tuccio, A. Giugni, A. Toma, C. Liberale, G. Das, F. Angelis, E. Fabrizio, and R. Zaccaria, "Molding of Plasmonic Resonances in Metallic Nanostructures: Dependence of the Non-Linear Electric Permittivity on System Size and Temperature," Materials **6**, 4879–4910 (2013).
27. H. Reddy, U. Guler, A. V. Kildishev, A. Boltasseva, and V. M. Shalaev, "Temperature-dependent optical properties of gold thin films," Optical Materials Express **6**, 2776 (2016).
28. V. P. Drachev, S. V. Perminov, S. G. Rautian, V. P. Safonov, and E. N. Khaliullin, "Polarization effects in silver nanoaggregates caused by local and nonlocal nonlinear-optical responses," J. Exp. Theor. Phys. **95**, 901–915 (2002).
29. A. V. Butenko, Y. E. Danilova, P. A. Chubakov, S. V. Karpov, A. K. Popov, S. G. Rautian, V. P. Safonov, V. V. Slabko, V. M. Shalaev, and M. I. Stockman, "Nonlinear optics of metal fractal clusters," Z. Phys. **17**, 283–289 (1990).
30. A. E. Ershov, A. P. Gavrilyuk, and S. V. Karpov, "Plasmonic nanoparticle aggregates in high-intensity laser fields: Effect of pulse duration," Plasmonics **11**, 403–410 (2015).
31. A. E. Ershov, A. P. Gavrilyuk, S. V. Karpov, and P. N. Semina, "Effect of local environment in resonant domains of polydisperse plasmonic nanoparticle aggregates on optodynamic processes in pulsed laser fields," Chin. Phys. B **24**, 47804 (2015).
32. A. E. Ershov, A. P. Gavrilyuk, S. V. Karpov, and S. P. Polyutov, "Restructuring of plasmonic nanoparticle aggregates with arbitrary particle size distribution in pulsed laser fields," Chin. Phys. B **25**, 117806 (2016).
33. Y. E. Danilova, N. N. Lepeshkin, S. G. Rautian, and V. P. Safonov, "Excitation localization and nonlinear optical processes in colloidal silver aggregates," Physica A **241**, 231–235 (1997).
34. R. A. Ganeev, A. I. Ryasnyansky, S. R. Kamalov, M. K. Kodirov, and T. J. Usmanov, "Nonlinear susceptibilities, absorption coefficients and refractive indices of colloidal metals," Physica D **34**, 1602 (2001).
35. S. V. Karpov, M. K. Kodirov, A. I. Ryasiyanskiy, and V. V. Slabko, "Nonlinear refraction of silver hydrosoles during their aggregation," Quantum Electronics **31**, 904–908 (2001).
36. N. N. Lepeshkin, W. Kim, V. P. Safonov, J. G. Zhu, R. L. Armstrong, C. W. White, R. A. Zhur, and V. M. Shalaev, "Optical nonlinearities of metal-dielectric composites," J. Nonlinear Opt. Phys. & Materials **8**, 191 (1999).
37. F. A. Zhuravlev, N. A. Orlova, V. V. Shelkovnikov, A. I. Plekhanov, S. G. Rautian, and V. P. Safonov, "Giant nonlinear susceptibility of thin films with (molecular j-aggregate)-(metal cluster) complexes," JETP Lett. **56**, 264–267 (1992).
38. S. V. Karpov, A. K. Popov, S. G. Rautian, V. P. Safonov, V. V. Slabko, V. M. Shalaev, and M. I. Shtokman, "Observation of a wavelength- and polarization-selective photomodification of silver clusters," JETP Lett. **48**, 571–573 (1988).
39. V. P. Safonov, V. M. Shalaev, V. A. Markel, Y. E. Danilova, N. N. Lepeshkin, W. Kim, S. G. Rautian, and R. L. Armstrong, "Spectral dependence of selective photomodification in fractal aggregates of colloidal particles," Phys. Rev. Lett. **80**, 1102–1105 (1998).

Optical Materials EXPRESS

40. S. V. Karpov, A. K. Popov, and V. V. Slabko, "Photochromic reactions in silver nanocomposites with a fractal structure and their comparative characteristics," Technical Physics **48**, 749–756 (2003).
41. Y. S. Barash, *Van der Waals Forces* (Nauka, Moscow, 1988).
42. J. N. Israelachvili, *Intermolecular and Surface Forces* (Academic Press, London, 1992).
43. L. D. Landau and E. Lifshitz, *Theory of Elasticity* (Butterworth-Heinemann, Oxford England Burlington, MA, 1986).
44. S. V. Karpov, I. L. Isaev, A. P. Gavrilyuk, V. S. Gerasimov, and A. S. Grachev, "General principles of the crystallization of nanostructured disperse systems," Colloid J. **71**, 313–328 (2009).
45. F. Claro and R. Rojas, "Novel laser induced interaction profiles in clusters of mesoscopic particles," Appl. Phys. Lett. **65**, 2743–2745 (1994).
46. V. A. Markel, L. S. Muratov, M. I. Stockman, and T. F. George, "Theory and numerical simulation of optical properties of fractal clusters," Phys. Rev. B **43**, 8183–8195 (1991).
47. G. Y. Panasyuk, J. C. Schotland, and V. A. Markel, "Short-distance expansion for the electromagnetic half-space green's tensor: general results and an application to radiative lifetime computations," J. Phys. A **42**, 275203 (2009).
48. W. C. Chew, *Waves and Fields in Inhomogeneous Media* (Van Nostrand Reinhold, New York, 1990).
49. B. T. Draine, "The discrete-dipole approximation and its application to interstellar graphite grains," Astrophys. J. **333**, 848–872 (1988).
50. V. A. Markel, L. S. Muratov, M. I. Stockman, and T. F. George, "Theory and numerical simulation of optical properties of fractal clusters," Phys. Rev. B **43**, 8183–8195 (1991).
51. V. A. Markel, V. M. Shalaev, E. B. Stechel, W. Kim, and R. L. Armstrong, "Small-particle composites. i. linear optical properties," Phys. Rev. B **53**, 2425–2436 (1996).
52. C. F. Bohren and D. R. Huffman, *Absorption and Scattering of Light by Small Particles* (John Wiley & Sons, New York, 1998).
53. V. A. Markel, V. M. Shalaev, E. B. Stechel, W. Kim, and R. L. Armstrong, "Small-particle composites. i. linear optical properties," Phys. Rev. B **53**, 2425–2436 (1996).
54. P. B. Johnson and R. W. Christy, "Optical constants of the noble metals," Phys. Rev. B **6**, 4370–4379 (1972).
55. J. C. Miller, "Optical properties of liquid metals at high temperatures," Philosophical Magazine **20**, 1115–1132 (1969).
56. C. Kittel, *Introduction to Solid State Physics* (John Wiley & Sons, Inc., New York, 1986), 6th ed.
57. M. Otter, "Temperaturabhängigkeit der optischen konstanten massiver metalle," Z. Phys. **161**, 539–549 (1961).
58. T. Castro, R. Reifenberger, E. Choi, and R. P. Andres, "Size-dependent melting temperature of individual nanometer-sized metallic clusters," Phys. Rev. B **42**, 8548–8556 (1990).
59. T. Castro, R. Reifenberger, E. Choi, and R. P. Andres, "Size-dependent melting temperature of individual nanometer-sized metallic clusters," Phys. Rev. B **42**, 8548–8556 (1990).
60. Y. A. Frenkel, *The Kinetic Theory of Liquids* (Nauka, Moscow, 1975).
61. O. Yeshchenko, I. Bondarchuk, V. Gurin, I. Dmitruk, and A. Kotko, "Temperature dependence of the surface plasmon resonance in gold nanoparticles," Surface Science **608**, 275 – 281 (2013).
62. D. Dalacu and L. Martinu, "Temperature dependence of the surface plasmon resonance of au/sio2 nanocomposite films," Appl. Phys. Lett. **77**, 4283–4285 (2000).
63. J. C. Miller, "Optical properties of liquid metals at high temperatures," Philosophical Magazine **20**, 1115–1132 (1969).
64. P. B. Johnson and R. W. Christy, "Optical constants of the noble metals," Phys. Rev. B **6**, 4370–4379 (1972).
65. V. A. Markel and A. K. Sarychev, "Propagation of surface plasmons in ordered and disordered chains of metal nanospheres," Phys. Rev. B **75**, 085426 (2007).
66. I. L. Rasskazov, S. V. Karpov, and V. A. Markel, "Surface plasmon polaritons in curved chains of metal nanoparticles," Phys. Rev. B **90**, 075405 (2014).
67. I. L. Rasskazov, S. V. Karpov, G. Panasyuk, and V. A. Markel, "Overcoming the adverse effects of substrate on the waveguiding properties of plasmonic nanoparticle chains," J. Appl. Phys. **119**, 043101 (2016).
68. I. L. Rasskazov, S. V. Karpov, and V. A. Markel, "Nondecaying surface plasmon polaritons in linear chains of silver nanospheroids," Opt. Lett. **38**, 4743–4746 (2013).

1. Introduction

Electromagnetic interactions in metal nanoparticles (NPs) are among the most intriguing phenomena in plasmonics [1] which are used in numerous breakthrough applications: optoelectronics [2–5], sensing [6–9], biomedicine [10]. Despite the fact that fundamental processes in plasmonics are well understood nowadays, there are some specific interactions where this understanding has not been reached yet and which give rise to emerging applications [11]. Interaction of NPs with high-intensity pulsed laser fields [12–14], plasmonic heating [15–17] and near-field heat transfer [18, 19] are among them.

In the paper [20], authors investigate theoretically, numerically and experimentally the tem-

Optical Materials EXPRESS

perature distribution in metal NPs excited by a modulated incoming light, the response in amplitude and phase of the temperature variations. Photothermal effects in colloidal NPs, including energy absorption by NPs, heat exchange with the environment and phase transitions of the particles and the environment are discussed in Ref. [21]. All of these processes are related to strong heating and even melting of NPs [22–24]. As a consequence, Q-factor of the NP surface plasmon resonance (SPR) considerably drops [25], which may dramatically change the physical pattern of interaction between NPs (single or aggregated) and electromagnetic radiation [26, 27]. Moreover, high-intensity light may cause mechanical effects due to interparticle forces. Therefore, the development of physical model which enables to describe interrelation between *electromagnetic*, *thermodynamic* and *mechanical* interactions in systems of NPs is of topical interest. Note that in alternative models the factor of suppression of SPR in heated NPs was not taken into account (see in particular [28]). However to get deep insight on the nature of processes in plasmonic colloidal aggregates experimentally studied earlier in [29] and subsequent publications (see below) we employed the optodynamical model proposed in [24] (its earlier version was published in [22]). We use the optodynamical model to study the interaction of pulsed laser radiation of different duration with mono- and polydisperse dimers and trimers composed of plasmonic nanoparticles as resonant domains of colloid Ag multiparticle aggregates [30]. In paper [31] we have analyzed how the local environment and the associated local field enhancement produced by surrounding particles affect the optodynamic processes in resonant domains of NP aggregates, including their optical properties. In [32] we have studied processes of interaction of pulsed laser radiation with resonant domains in Ag colloidal aggregates with different interparticle gaps and particle size distributions.

Nonlinear optical effects observed in nanocolloids with silver and gold NP aggregates included four-wave mixing of pulsed laser radiation [29], nonlinear optical activity (nonlinear gyrotropy), spontaneous rotation of the polarization ellipse [28], non-linear absorption and refraction [33–35], the reverse Faraday effect [28], the optical Kerr effect [36], harmonics generation [34], enhancement of nonlinear responses of organic molecules adsorbed on nanoparticle surfaces [37] and optical memory [38–40]. In the paper [39] authors report on a record in composite medium containing large colloidal Ag aggregates of pulsed laser radiation with five different wavelengths of visible and near IR range in one irradiated spot.

In this paper, we summarize our previous and new results regarding thermal effects in single and aggregated NPs in high-intensity pulsed laser fields. We show how thermal effect may lead to new phenomena changing the usual pattern of light interaction with systems of bound plasmonic nanoparticles.

2. Model

We have developed combined physical model which thoroughly describes interaction between pulsed laser radiation and metal NP aggregates. Basic interactions in such systems can be divided into three major parts: mechanical, electrodynamical and thermodynamical. It is obvious that each of these parts is well known and developed, however implementation of above mentioned interactions into one combined model opens the opportunity to describe vast majority of various phenomena in aggregates of NPs.

2.1. Mechanical interactions

Let us start with simple mechanical part which is based on the motion equations. Consider the aggregate of N spherical NPs. In general case, each NP in aggregate moves under the influence of van der Waals $\mathbf{F}_{\mathrm{vdw}}$, viscous $\mathbf{F}_{\mathrm{v}}$ and light-induced optical forces $\mathbf{F}_{\mathrm{opt}}$. Moreover, we consider interparticle friction $\mathbf{F}_{\mathrm{f}}$ and elastic $\mathbf{F}_{\mathrm{el}}$ forces to take into account interaction between touching NPs. The motion of i-th NP (where $i = 1, 2, \ldots, N$) with mass m_i can be characterized by the

Optical Materials EXPRESS

following expression:

$$m_i \ddot{\mathbf{r}}_i = (\mathbf{F}_{\text{vdw}})_i + (\mathbf{F}_{\text{el}})_i + \left(\mathbf{F}_{\text{opt}}\right)_i + (\mathbf{F}_{\text{v}})_i + (\mathbf{F}_{\text{f}})_i, \tag{1}$$

where $\mathbf{r}_i$ denotes the position of i-th NP center of mass and double dot over the vector denotes the time derivative. In this paper, we provide general expressions and brief explanation of these interactions. More comprehensive study can be found in Ref. [24].

Now, let us describe each force from eq. (1) more specifically. The pair potential energy of the van der Waals interaction between i-th and j-th NPs is described by well-known expression [41]:

$$(U_{\text{vdw}})_{ij} = -\frac{A_{\text{H}}}{6}\left(\frac{2R_iR_j}{h_{ij}^2 + 2R_ih_{ij} + 2R_jh_{ij}} + \frac{2R_iR_j}{h_{ij}^2 + 2R_ih_{ij} + 2R_jh_{ij} + 4R_iR_j} + \right.$$
$$\left. + \ln\frac{h_{ij}^2 + 2R_ih_{ij} + 2R_jh_{ij}}{h_{ij}^2 + 2R_ih_{ij} + 2R_jh_{ij} + 4R_iR_j}\right), \tag{2}$$

where R is the radius of spherical NP; $h_{ij} = |\mathbf{r}_{ij}| - (R_i + R_j)$ is the interparticle gap, $\mathbf{r}_{ij} = \mathbf{r}_i - \mathbf{r}_j$; A_H is the Hamaker constant [42]. Therefore, one should take into account the interaction of i-th with the rest of aggregate to get $(\mathbf{F}_{\text{vdw}})_i = -\sum_{j=1, j\neq i}^{N} \partial(U_{\text{vdw}})_{ij}/\partial\mathbf{r}_i$.

The solution of Hertz problem for deformation of two touching spheres [43] can be utilized to determine potential energy of elastic interaction between two touching NPs with adsorption layers (neglecting the Poisson's ratio) [43, 44]:

$$(U_{\text{el}})_{ij} = \frac{8}{15}\left(h_i + h_j - h_{ij}\right)^{5/2}\left[\frac{(R_i + h_i)(R_j + h_j)}{R_i + h_i + R_j + h_j}\right]^{1/2}\frac{(E_{\text{el}})_i \cdot (E_{\text{el}})_j}{(E_{\text{el}})_i + (E_{\text{el}})_j}H(h_i + h_j - h_{ij}). \tag{3}$$

Here h is the thicknesses of unstrained NP's adsorption layer; E_{el} is the elasticity modulus of NP adlayer; $H(x)$ is the Heaviside function. Thus, taking into account interaction of i-th NP with other NPs contacting therewith, one can obtain total elastic force $(\mathbf{F}_{\text{el}})_i = -\sum_{j=1, j\neq i}^{N} \partial(U_{\text{el}})_{ij}/\partial\mathbf{r}_i$.

Next, assume that laser pulse with duration τ irradiates NP aggregate. Then, the potential energy of such optical interaction between NP aggregate and incident excitation can be found as follows [45]:

$$U_{\text{opt}} = -\frac{1}{4}\text{Re}\sum_{i=1}^{N}\left[\mathbf{d}_i \cdot \mathbf{E}^*(\mathbf{r}_i) + \frac{1}{2}\mathbf{d}_i \cdot \left(\frac{\mathbf{d}_i}{\varepsilon_0\alpha_i} - \mathbf{E}(\mathbf{r}_i)\right)^* - \varepsilon_0\alpha_i|\mathbf{E}_0|^2\right] \cdot H(\tau - t). \tag{4}$$

Here $\mathbf{d}_i$ is the dipole moment which is induced on i-th NP; $\mathbf{E}(\mathbf{r}_i)$ is the strength of external electromagnetic field at $\mathbf{r}_i$ point, $\mathbf{E}_0$ is the amplitude of the field; α_i is the dipole polarizability of the i-th particle and symbol $(*)$ denotes complex conjugate. Optical force $(\mathbf{F}_{\text{opt}})_i$ which acts on i-th NP can be found by simple derivation of eq. (4): $(\mathbf{F}_{\text{opt}})_i = -\partial U_{\text{opt}}/\partial\mathbf{r}_i$.

Viscous friction forces acting on i-th NP moving in a viscous medium with the velocity $\mathbf{v}_i$ obeys the Stokes law:

$$(\mathbf{F}_{\text{v}})_i = -6\pi\eta(R_i + h_i)\mathbf{v}_i, \tag{5}$$

where η is the dynamical viscosity of the interparticle medium.

Finally, we consider tangential friction force which occurs when NPs in aggregate move transversally relative to each other. Such interaction can be described by analogy with the forces of dry friction (although they are not the ones). The coefficient of friction is an effective parameter that characterizes the degree of interaction between the touching NP's adlayers. The effective friction coefficient can significantly exceed unity due to strong intermolecular interaction of NP's adlayers and their non-uniform deformation. The direction of tangential friction force

Optical Materials EXPRESS

is opposite to the projection of the relative velocity of particles $(\mathbf{v}_i - \mathbf{v}_j)$ on the plane of adlayers contact. Thus, the tangential friction force exerted on the i-th NP by the j-th NP is determined by the following expression:

$$(\mathbf{F}_\mathrm{f})_i = -\mu \sum_{\substack{j=1 \\ j\neq i}}^{N} \left|(\mathbf{F}_\mathrm{el})_{ij}\right| \mathbf{q}_{ij}. \tag{6}$$

Here μ is the effective friction coefficient; $\mathbf{q}_{ij}$ is the normalized vector of the projection of particles relative velocity on the plane of contact of particle adlayers:

$$\mathbf{q}_{ij} = \frac{(\mathbf{v}_j - \mathbf{v}_i) - \mathbf{n}_{ij}\left((\mathbf{v}_j - \mathbf{v}_i)\cdot \mathbf{n}_{ij}\right)}{\left|(\mathbf{v}_j - \mathbf{v}_i) - \mathbf{n}_{ij}\left((\mathbf{v}_j - \mathbf{v}_i)\cdot \mathbf{n}_{ij}\right)\right|},$$

where $\mathbf{n}_{ij} = \mathbf{r}_{ij}/|\mathbf{r}_{ij}|$.

2.2. Electrodynamical interactions

Electrodynamical part is based on the coupled dipole approximation [46], which allows one to calculate the electromagnetic interactions between NPs, incident radiation and a substrate [47].

Let us consider the aggregate of NPs in host medium with permittivity ε^M which is illuminated by electromagnetic plane wave $\mathbf{E}(\mathbf{r}) = \mathbf{E}_0 \exp(i\mathbf{k}\cdot\mathbf{r})$. Here $|\mathbf{k}| = 2\pi\sqrt{\varepsilon^\mathrm{M}}/\lambda$ is the wave vector, $\mathbf{E}_0$ is the amplitude of the electric component of the electromagnetic field. In general case, incident plane wave does not excite all NPs in the aggregate. We introduce coefficient κ_i to take this fact into account, where $\kappa_i = 1$ for i-th nanoparticle which is excited by incident field and $\kappa_i = 0$ otherwise. In this case, the dipole moment $\mathbf{d}_i$ induced on the i-th NP can be described by following equation [46]:

$$\mathbf{d}_i = \varepsilon_0 \alpha_i \left[\mathbf{E}(\mathbf{r}_i)\,\kappa_i + \sum_{j\neq i}^{N} \hat{\mathbf{G}}(\mathbf{r}_i, \mathbf{r}_j)\mathbf{d}_j\right], \tag{7}$$

where α_i is the dipole polarizability of the i-th NP, $\hat{\mathbf{G}}(\mathbf{r}_i, \mathbf{r}_j)$ is the 3×3 Green's interaction tensor that describes the electric field produced at $\mathbf{r}_i$ by electric dipole $\mathbf{d}_j$ located at $\mathbf{r}_j$. Expressions for $\hat{\mathbf{G}}(\mathbf{r}_i, \mathbf{r}_j)$ can be found elsewhere [48].

Finally, the dipole polarizability of i-th NP which takes into account the radiation reaction correction [49], has the form [50]:

$$\alpha_i^{-1} = [\alpha_i^{(0)}]^{-1} - \frac{i}{6\pi}|\mathbf{k}|^3, \tag{8}$$

where $\alpha_i^{(0)}$ is so-called bare or Lorenz-Lorentz quasistatic polarizability of the particle.

For the extinction efficiency of a particle ensemble surrounded by other particles we have the formula [51] (for a single particle, averaging over ensemble is omitted):

$$Q_\mathrm{e} = \frac{\sigma_\mathrm{e}}{\sum\limits_{i=1}^{N} \pi R_i^2}. \tag{9}$$

Here the extinction cross section is given by the equation

$$\sigma_\mathrm{e} = 4\pi\,|\mathbf{k}|\,\mathrm{Im}\sum_{i=1}^{N} \frac{(\mathbf{d}_i \cdot \mathbf{E}^*(\mathbf{r}_i))}{|\mathbf{E}_0|^2}. \tag{10}$$

Optical Materials EXPRESS

2.3. Thermal effects

The key effect which should be taken into account to describe the impact of thermal effects on optical response of NP is variation of NPs permittivity under conditions of their strong heating, e.g. in high-intensity pulsed laser field. In our work, we take into consideration the fact that a particle can be in the melting process. Thus, the heated NP is considered as a core-shell nanosphere with a solid core and a liquid shell. Therefore, the $\alpha_i^{(0)}$ can be described as follows [52]:

$$\alpha_i^{(0)} = 4\pi R_i^3 \times \frac{\left(\varepsilon_i^{\mathrm{L}} - \varepsilon^{\mathrm{M}}\right)\left(\varepsilon_i^{\mathrm{S}} + 2\varepsilon_i^{\mathrm{L}}\right) + f_i\left(\varepsilon_i^{\mathrm{S}} - \varepsilon_i^{\mathrm{L}}\right)\left(\varepsilon^{\mathrm{M}} + 2\varepsilon_i^{\mathrm{L}}\right)}{\left(\varepsilon_i^{\mathrm{L}} + 2\varepsilon^{\mathrm{M}}\right)\left(\varepsilon_i^{\mathrm{S}} + 2\varepsilon_i^{\mathrm{L}}\right) + 2f_i\left(\varepsilon_i^{\mathrm{S}} - \varepsilon_i^{\mathrm{L}}\right)\left(\varepsilon_i^{\mathrm{L}} - \varepsilon^{\mathrm{M}}\right)}. \tag{11}$$

Here $\varepsilon_i^{\mathrm{S}}$ and $\varepsilon_i^{\mathrm{L}}$ are the temperature and size dependent permittivities of the particle material in the solid and liquid state, respectively, f_i is the mass fraction of solid material in the particle. The expression (11) takes into account the extreme cases of completely solid ($f_i = 0$) and fully liquid particles ($f_i = 1$). The full description of f_i will be given below. It should be noticed that metal NP keeps its spherical shape even in the fully liquid state due to extremely high values of surface tension. Therefore, the expression (11) is valid for any values of f_i.

Permittivities $\varepsilon_i^{\mathrm{S}}$ and $\varepsilon_i^{\mathrm{L}}$ take into account finite size effects (FSE) [53] and temperature dependence of optical constants:

$$\varepsilon_i^{\mathrm{S,L}} = \varepsilon_{\mathrm{tab}}^{\mathrm{S,L}} + \frac{\omega_{\mathrm{pl}}^2}{\omega\left(\omega + i\Gamma_0\right)} - \frac{\omega_{\mathrm{pl}}^2}{\omega\left(\omega + i\Gamma_i\right)}, \tag{12}$$

where ω is the electromagnetic field frequency, $\varepsilon_i^{\mathrm{S,L}}$ is the permittivity of the solid or liquid material of the particles, $\varepsilon_{\mathrm{tab}}^{\mathrm{S,L}}$ is the corresponding tabulated experimental values for bulk at the temperature of 300 K for solid material [54] and at the melting point for liquid one [55], Γ_0 is the time dependent bulk electron relaxation constant for corresponding temperature, ω_{pl} is the plasma frequency of the particle material, Γ_i is the temperature and size dependent electron relaxation constant of a particle:

$$\Gamma_i = \Gamma_0\left(T_i^{\mathrm{ion}}\right) + A\frac{\mathrm{v_F}}{R_i}. \tag{13}$$

Here $\mathrm{v_F}$ is the Fermi velocity and T_i^{ion} is the temperature of ion component. The value of A is taken to be unit in most of cases [52]. However, the relaxation processes depend on the state of particle surface and on other factors. The dependence of the relaxation constant for solid bulk material $\Gamma_0(T)$ on the temperature can be approximated by the following expression [56]:

$$\Gamma_0(T) = bT + c, \tag{14}$$

where b and c are the linear dependence coefficients obtained by linear approximation of the experimental data [57] (detailed discussion will be published elsewhere).

Description of thermodynamical processes is based on a two-component model, that considers the temperature variations of the conduction electron and ion (crystal lattice) components of each NP. The model takes into account heating of the electron component by incident optical radiation, heat transfer between the electron and ion components, heat exchange between the ion component and the environment [22,24], as well as size dependence of NP's melting point [58].

The temperature of the electron subsystem T_i^{e} which depends on the absorption of radiation energy by nanoparticle and on heat exchange with the crystal lattice (ion subsystem) is described by the following expression [22]:

$$C_i^{\mathrm{e}}\frac{dT_i^{\mathrm{e}}}{dt} = -g\left[T_i^{\mathrm{e}} - T_i^{\mathrm{ion}}\right] + \frac{W_i}{V_i}, \tag{15}$$

Optical Materials EXPRESS

where $C_i^{\mathrm{e}} = 68T_i^{\mathrm{e}}$ J · m^{-3} · K^{-1} is the volumetric heat capacity, V_i is the volume of a spherical particle, $g = 4 \times 10^{16}$ J · m^{-3} · K^{-1} is the energy exchange rate between electron and ion subsystems, W_i is the radiation power absorbed by the particle. In dipole approximation, W_i can be found using the equation [24]:

$$W_i = \frac{\omega |\mathbf{d}_i|^2}{2\varepsilon_0} \mathrm{Im}\left(\frac{1}{\alpha_i^*}\right), \tag{16}$$

where asterisk denotes the complex conjugate.

Developed model takes into account the phase transition at the melting point of the particle. Therefore, the heat exchange between ion component of the particle with its electronic component and the environment is described in terms of the amount of heat Q_i^{ion} which is absorbed by a particle [22]:

$$\frac{dQ_i^{\mathrm{ion}}}{dt} = gV_i \left[T_i^{\mathrm{e}} - T_i^{\mathrm{ion}}\right] + \upsilon_i, \tag{17}$$

where υ_i is the rate of heat transfer between particle and its environment. The temperature of the ion subsystem of a particle during the melting process is described as follows [24]:

$$T_i^{\mathrm{ion}} = \begin{cases} \dfrac{Q_i^{\mathrm{ion}}}{C_i^{\mathrm{ion}} V_i}, & \text{when } Q_i^{\mathrm{ion}} < Q_i^{(1)} \\ T_i^{\mathrm{L}}, & \text{when } Q_i^{(1)} \le Q_i^{\mathrm{ion}} \le Q_n^{(2)} \\ \dfrac{Q_i^{\mathrm{ion}} - LV_i}{C_i^{\mathrm{ion}} V_i}, & \text{when } Q_i^{\mathrm{ion}} > Q_i^{(2)}. \end{cases} \tag{18}$$

Here L is the volumetric heat of fusion, C_i^{ion} is volumetric heat capacity of the ion subsystem of the i-th particle material, $T_i^{\mathrm{L}} = T^{\mathrm{L}}(R_i)$ is the size dependent melting temperature [59], $Q_i^{(1)}$ is the heat that corresponds to the onset of the particle melting:

$$Q_i^{(1)} = C_i^{\mathrm{ion}} V_i T_i^{\mathrm{L}}, \tag{19}$$

and $Q_i^{(2)}$ is the heat that corresponds to the end of particle's melting process:

$$Q_i^{(2)} = Q_i^{(1)} + LV_i. \tag{20}$$

Thus, we can determine the mass fraction f_i of the molten material in equation (11) as follows:

$$f_i = \begin{cases} 0, & \text{when } Q_n^{\mathrm{ion}} < Q_i^{(1)} \\ \dfrac{Q_i^{\mathrm{ion}} - Q_i^{(1)}}{C_i^{\mathrm{ion}} V_i}, & \text{when } Q_i^{(1)} \le Q_i^{\mathrm{ion}} \le Q_i^{(2)} \\ 1, & \text{when } Q_i^{\mathrm{ion}} > Q_i^{(2)} \end{cases}. \tag{21}$$

The rate of heat transfer from a particle to the environment can be found using the following expression [43]:

$$\upsilon_i = -\varkappa \int_{S_i} \nabla T(\mathbf{r}, t) \cdot \mathbf{n} dS. \tag{22}$$

Here $\varkappa$ and $T(\mathbf{r}, t)$ are coefficients of thermal conductivity and the temperature of host medium, correspondingly, and $\mathbf{n}$ is the normal vector to the particle surface. The integration is performed

Optical Materials EXPRESS

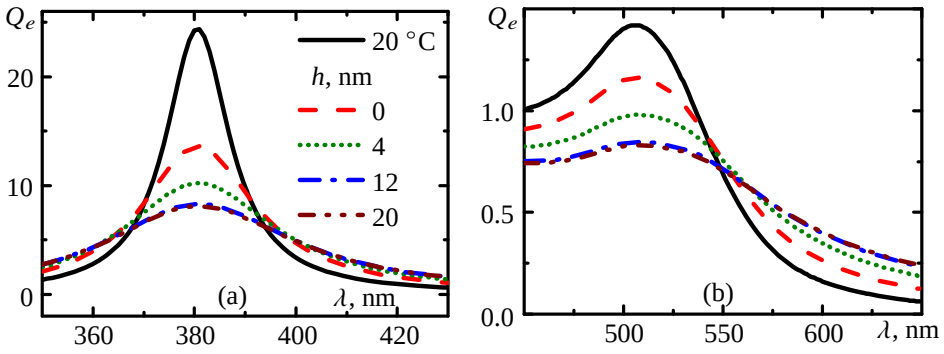

Fig. 1. Extinction spectra of Ag — (a) and Au — (b) NPs with 20 nm radius at room (20 °C, solid line) and melting (≈ 1064 °C) temperatures for different values of liquid shell thicknesses h. Dielectric constant of the environment is $\varepsilon_h = 1.78$. The spectral range on graphs is limited by experimental data for optical constants of liquid metals [57].

over the surface S_i of the i-th particle. The rate of heat exchange due to the radiation is much less than due to the thermal conductivity so that the first one is omitted in this model.

The heat equation for the environment surrounding a particle is solved to determine the values of $T(\mathbf{r}, t)$:

$$\frac{\partial T(\mathbf{r}, t)}{\partial t} = a\Delta T(\mathbf{r}, t), \tag{23}$$

where a is the thermal diffusivity of the environment material.

The particle and the interparticle medium are heated when laser radiation is absorbed that results in a change of the adlayer elasticity modulus due to destruction of molecular bonds in the polymer grid of the adlayer. This occurs over finite relaxation time τ_r and is described by the expression [6, 44]:

$$\tau_{\mathrm{r}}(T) = \tau_0 \exp\left(\frac{U_{\mathrm{f}}}{k_{\mathrm{B}}T}\right). \tag{24}$$

The value of τ_0 is assumed to be 10^{-12} s which is characteristic vibration period of atoms in molecules [22,60], U_{f} is the energy of chemical bonds in the polymer adlayer (taken to be about 1 eV in our calculations, which is typical for the chemical bond energy of polymers). Taking into account the finite relaxation time, the temperature dependence of the elasticity modulus is described by the following equation [22]:

$$\frac{d(E_{\mathrm{el}})_i}{dt} = -\frac{(E_{\mathrm{el}})_i}{\tau_{\mathrm{r}}((T_{\mathrm{m}})_i)}, \tag{25}$$

where $(T_{\mathrm{m}})_i$ is the average temperature of the heated area near the i-th particle.

3. Results

3.1. Thermal effects in single spherical nanoparticle

Let us start with the temperature dependence of SPR in isolated metal NP. As it was shown previuosly, the heating process in Au and Ag NPs [61] or thin films [27, 62] can considerably affect both the peak magnitude of SPR and position of its maximum. Here we present an extensive consideration of the melting process in single NP. Figure 1 shows the extinction spectra $Q_e(\lambda)$ of liquid-shell/solid-core Ag and Au NPs with different core-to-shell ratio. Values of

Optical Materials EXPRESS

liquid metal permittivity at the melting temperature were taken for gold in Ref. [57] and for silver — from Ref. [63]; at room temperature for gold — from [57] and [64], and for silver — from [64]. It is clearly seen that SPR of NPs is strongly suppressed during the melting process. Strong heating of NPs is accompanied by increasing scattering of electrons at the crystal lattice defects (vacancies, dislocations, grain boundaries). This explains the significant increase of the relaxation constant for conduction electrons at the melting point.

Our experiment on manifestation of heating and melting of Au NPs is described in detail in [25]. Compared to silver, gold NPs are resistant to oxidation even in the temperature range slightly above the melting point. Therefore, in our work [25] we studied annealed Au NPs deposited on quartz substrate. These NPs do not undergo further changes during several heating cycles up to the melting point.

In Ref. [61], Au NPs were heated to temperatures below the melting point which leads to a broadening of SPR and a decrease of its amplitude. In [62], the same effect was observed at the melting point of Au NPs with 2 nm, 8 nm and 15 nm radii. However considerable contribution of FSE can overcome the suppression of SPR due to heating in these cases. To get rid of undesirable manifestation of FSE, we experimentally study NPs with much larger size, namely ≈ 56 nm. In this case FSE is nearly negligible.

Experimentally obtained data in [25] shows evolution of the extinction spectrum of Au NPs during temperature growth beyond the melting point up to 1120 °C. It was shown that the NP temperature growth results in the gradual decrease of a SPR amplitude. The complete suppression of SPR corresponds to the temperature 1120 °C.

3.2. Photochromic effects in disordered nanoparticle aggregates

Now we turn to practical applications of pulsed laser interaction with disordered colloidal NP aggregates. We discuss how suppression of SPR in melting NPs can change interactions of radiation with the systems of bound NPs. Colloidal plasmonic aggregates formed in disperse systems are certainly one of the most popular objects for experimental research. For better understanding of such processes, it is worthwhile to consider light interaction with resonant domains of such aggregates. Resonant domain represents a group of several bound NPs. Such groups are randomly distributed over a large aggregate which in turn is composed of several thousands or more NPs [24]. Each frequency of inhomogeneously broadened plasmonic spectrum of such aggregate corresponds to resonant frequency of individual set of domains comprising the aggregate. Interaction of disordered NP aggregates with monochromatic high-intensity pulsed laser radiation can be accompanied either by solid-liquid state transition of NPs and subsequent sharp decrease of the SPR Q-factor or by structural changes in different resonant domains [39, 40]. Both these changes result in instant formation of narrow dips in absorption spectrum. The latter means that disordered colloidal NP aggregates manifest photochromic effects.

Figure 2 shows numerical results based on the model [24] for modification processes in multiparticle Ag aggregates exposed to monochromatic pulsed laser radiation, which strictly speaking for the first time reproduce experimental data on this effect [39, 40]. The physical model proposed in our work provides us with opportunity to obtain further insight into the physical nature of the processes underlying photochromic effects. We show that these effects can be divided into dynamic and long-term types, which have different nature. Figure 2(a) shows the dynamic effect which occurs during the pulse duration and caused by melting of NPs in resonant domains without changes of interparticle distance. Positions of resonant domains in disordered aggregate composed of 3000 Ag NPs and excited by incident radiation with different wavelengths 450 and 650 nm are shown in Fig. 2(c),(d). These figures show that we have different set of domains spatially separated from each other (in 3D aggregate some of domain particles are partially obscured by other NPs).

The kinetics of dynamic effects under picosecond pulsed radiation was studied in [24] and

Optical Materials EXPRESS

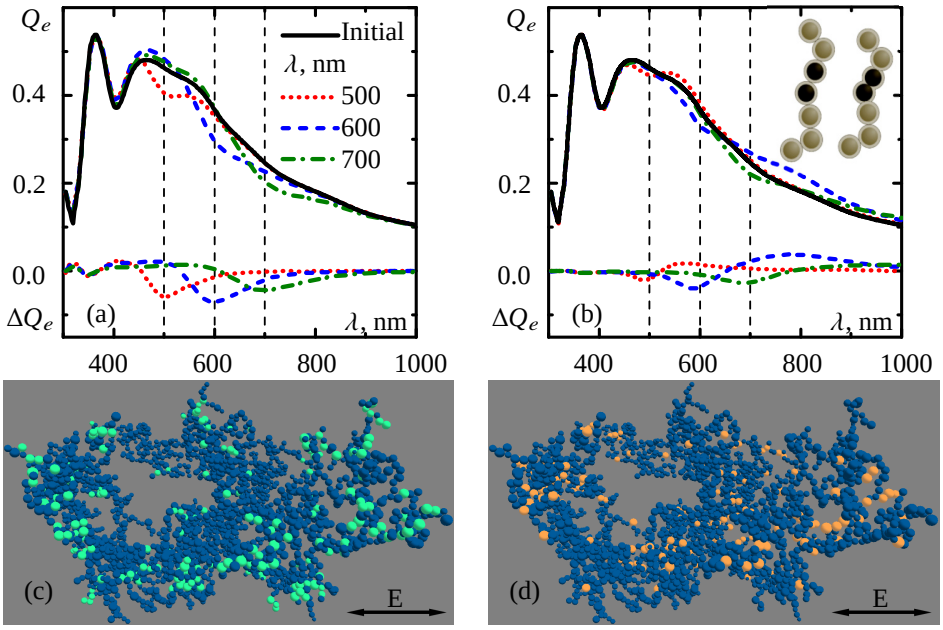

Fig. 2. (a), (b) — changes in extinction spectra $Q_e(\lambda)$ and differential spectra $\Delta Q_e(\lambda) = (Q_e)_{in} - (Q_e)_a$ of monodisperse Ag NP aggregate excited by pulsed radiation with 20 ps pulse duration and $I = 2.4 \times 10^8$ W·cm^{-2} intensity (here $(Q_e)_{in}$ is initial extinction, $(Q_e)_a$ is extinction after irradiation); vertical dashed lines indicate excitation wavelengths. (a) — at the end of a pulse (dynamic effect), (b) — in 40 ns after a pulse (long-term effect); changes in resonant domain are shown in inset (b) (see the description in the text). NP aggregates were simulated with molecular dynamics method described in [24]. (c),(d) — positions of resonant domains in 3D aggregate consisting of $N = 3000$ Ag NPs with resonant wavelengths 450 nm (c) and 650 nm (d); polarization of incident field is indicated by arrows (in both cases 200 nanoparticles are highlighted).

characteristic time was about 20 ps. After the pulse is over, NP becomes solid again. In picosecond laser pulses, due to inertia of NPs, they do not have enough time to change their positions in domains during the laser pulse neither under the action of the van der Waals forces nor under the light-induced interaction. At such time scales, changes in the extinction spectra caused only by the suppression of resonant properties of melted NPs which give rise to fast nonlinear optical response of the NP aggregate [24].

Figure 2(b) shows the long-term photochromic effect. It is related to restructuring of resonant domains caused by melting of NP polymer adsorption layers (1–2 nm thick) and degradation of their elasticity due to contact with hot metal NP core. It results in consequent shift of adjacent NPs in domains to each other up to contact of their metal cores. Kinetics of such process under nanosecond pulsed radiation was investigated in [24] and characteristic time exceeded 1–2 ns. Therefore, in the case of nanosecond pulsed laser radiation, the nonlinear response is associated with restructuring of resonant domains. The inset in Figure 2(b) shows the fragment of aggregate with a two-particle resonant domain (marked dark) before (left) and after (right) its photo-induced modification. This modification is accompanied by approaching the particles to each other due to deformation of adlayers. Note, that in nanosecond time scale the decreased absorption in plasmonic spectrum within a dip is accompanied by increased absorption in the long wavelength region adjacent to the dip. After the action of nanosecond pulses minor spectral changes may continue in the later stages. Thus, after a pulsed laser irradiation with different

Optical Materials EXPRESS

wavelengths, plasmonic absorption spectrum of disordered colloidal NP aggregates may acquire several dips exactly at the radiation wavelengths. These dips clearly demonstrates the spectral selectivity of the modification process. Visual effect after radiation is that the region of the sample exposed to laser pulse acquires the color and polarization of the incident radiation. This effect demonstrates a polarization selectivity because radiation with different linear polarizations interacts with individual set of domains even at the same wavelengths [40].

3.3. Thermal effects in ordered nanostructures

Now we consider interaction of pulsed laser radiation with ordered nanostructures. To this end, we study optical plasmonic waveguides (OPW) in the form of plasmonic NP chains [65, 66] which attract significant attention due to their applicability for transmission of modulated optical radiation by means of surface plasmon polaritons (SPP). A great number of publications underlines the interest in this objects. But never before the effect of strong heating of nanoparticles in the OPW was studied. In the meanwhile, practical employment of OPWs without providing them with cooling device will be limited.

From practical point of view, OPW is considered to be fabricated on some substrate instead of free space. Thus, Green's tensor in eq. (7) will be described as follows:

$$\hat{\mathbf{G}}(\mathbf{r}_i, \mathbf{r}_j) = \hat{\mathbf{G}}_{\text{free}}(\mathbf{r}_i, \mathbf{r}_j) + \hat{\mathbf{G}}_{\text{refl}}(\mathbf{r}_i, \mathbf{r}_j), \tag{26}$$

where $\hat{\mathbf{G}}_{\text{free}}(\mathbf{r}_i, \mathbf{r}_j)$ and $\hat{\mathbf{G}}_{\text{refl}}(\mathbf{r}_i, \mathbf{r}_j)$ are Green's tensors that describe electric field in a homogeneous environment and reflected from the substrate, correspondingly. More comprehensive discussion of eq. (26) can be found in [67].

Consider the simplest case of a linear chain consisting of $N = 11$ identical spherical Ag NPs with 8 nm radius. NPs are arranged equidistantly in the host medium with permittivity 1.78 over the surface of the quartz substrate (see Fig. 3). Here we use spherical NPs just to demonstrate thermal effects. The papers [65, 68] show that the use of NPs in the form of prolate or oblate spheroids can dramatically increase the transmission efficiency. The substrate keeps constant temperature 20 °C. The distance between the centers of the neighboring particles is 24 nm. We assume that only the first ($i = 1$) locally excited NP interacts with an incident radiation which is conventional condition for numerical study of OPW in publications (see in particular [65, 66]). Experimentally it can be implemented by using, for example, a near-field scanning optical microscope (NSOM) tip. Thus, transmission properties of OPW can be described by the transmission coefficient [65, 66, 68]:

$$Q_{\text{tr}} = \frac{|\mathbf{d}_N(t)|}{|\mathbf{d}_1(t=0)|}, \tag{27}$$

where $\mathbf{d}_N(t)$ and $\mathbf{d}_1(t = 0)$ are oscillation amplitudes of dipole moments induced on the last (at arbitrary moment of time) and the first (at initial moment of time) particles, correspondingly. The impact of thermal effects on SPP propagation is very important factor for such type of OPW excitation. However temperature dependence of NP's dielectric constants is usually overlooked in most studies. In our work we used a finite element method in original realization for calculations of temperature distribution around OPW.

It is obvious that thermal effects in OPW should strongly depend on the intensity I of incident laser radiation. For low I magnitudes, none of NPs will reach the melting point. However in this case, it will be nearly impossible to register optical signal at the end of OPW due to strong SPP attenuation. For high values of I, we will observe extreme heating of OPW NPs. In this case, their resonant properties will be dramatically suppressed. Therefore, we consider the case of intermediate magnitude of intensity between these two extreme cases. Our calculations show that for $I = 1.57 \times 10^8$ W $\cdot$ cm^{-2}, only first NP reaches the melting point. We expect that Q_{tr} will not drop dramatically in this case.

Optical Materials EXPRESS

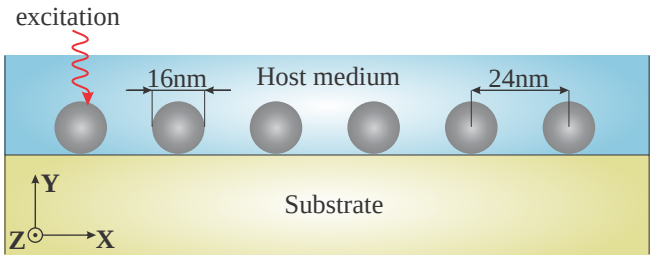

Fig. 3. The OPW geometry used in numerical simulations.

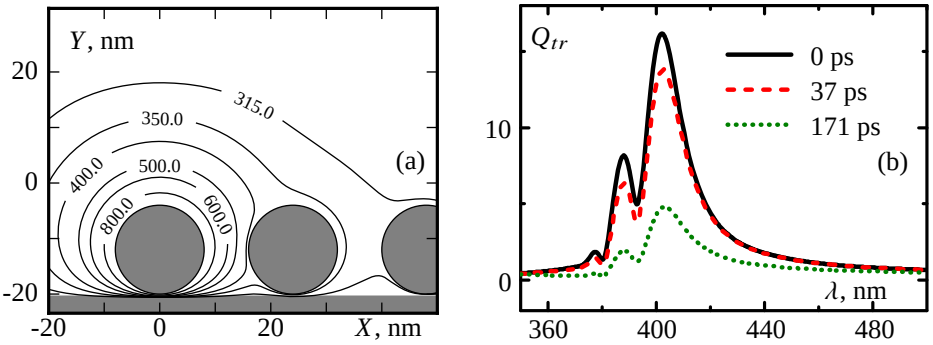

Fig. 4. The temperature T distribution at $t = 1$ ns for first three OPW Ag NPs. Wavelength $\lambda = 402$ nm and polarization along the X axis — (a). Transmission spectra of the OPW at different moments of time: the initial moment of time (solid line); the beginning of $i = 1$ NP melting (dashed line); the end of $i = 1$ NP melting (dotted line) — (b).

Figure 4(a) represents XOY-plane ($z = 0$) temperature distribution in the OPW at the end of the 1 ns pulse irradiation. We can see that only first three particles are significantly heated, and the temperature of the $i = 1$ particle reaches the melting point. We take into account heat exchange between NPs through environment and between a NP chain and thermally stable substrate.

Transmission spectra of OPW at different stages of $i = 1$ particle melting process are shown on Fig. 4(b). The OPW transmission spectrum slightly changes when the $i = 1$ NP reaches the melting temperature ($T \approx 1080$ K for NP with 8 nm radius, dash line). This change is associated with the change of the dielectric constant of the particle material. It should be noticed that NP is still in the solid state at 37 ps. However significant suppression of SPR in the $i = 1$ NP occurs when it becomes fully liquid at 171 ps moment of time (the end of the first NP melting process). It is clearly seen that OPW transmission efficiency drops threefold in this case (dotted line). As a consequence, the transmitted energy is also reduced. In turn, it results in a decrease of absorbed energy and the temperature of the second and subsequent NPs. The further increase of NP temperature in a chain occurs due to heat exchange between them, between NPs and host medium including substrate.

4. Conclusion

To conclude, we have developed experimentally verified combined theoretical model that describes light-induced dipole interactions between NPs and surrounding medium in high-intensity optical fields. This model takes into account vast majority of various physical phenomena that take place in different systems of bound NPs. The interactions in NP aggregates

Optical Materials EXPRESS

cover three major group of the processes: mechanical, electrodynamical, thermal. The melting processes in Au and Ag NPs have been studied numerically and experimentally [25]. Our experimental results evidence the validity of the proposed model. It was shown that the melting of plasmonic NP sufficiently suppresses its SPR. The developed model was used to reproduce numerically photochromic effects in disordered colloidal Ag NP aggregates observed experimentally. Strong heating of NPs in resonant domains of aggregates explains dynamic and long-term laser photochromic effects which have application potential in data storage devices. Finally, we have shown that thermal effects significantly impair the transmission efficiency of OPW due to suppression of the NP resonant properties and deterioration of SPR Q-factor. Optimal conditions for stable waveguiding through OPW are limited by an intensity and wavelength of incident pulsed laser radiation. We also conclude that technological substrates for OPWs must be provided with cooling devices.

5. Acknowledgments

This work was performed within the State contract of the RF Ministry of Education and Science for Siberian Federal University for scientific research in 2017–2019 and SB RAS Program No II.2P (0358-2015-0010). The calculations were performed using the MVS-1000 M cluster at the Institute of Computational Modeling, Federal Research Center KSC SB RAS.